Tunable magnetic properties of transition metal doped MoS$_2$

Antonis N. Andriotis[*]

Institute of Electronic Structure and Laser, FORTH, P.O. Box 1527, 71110 Heraklio, Crete, Greece

Madhu Menon[†]

Department of Physics and Astronomy, University of Kentucky, Lexington, Kentucky 40506-0055, USA
and Center for Computational Sciences, University of Kentucky, Lexington, Kentucky 40506-0045, USA

We report a detailed investigation of the electronic and magnetic properties of the transition metal (TM) doped two-dimensional (2D) MoS$_2$ using *ab initio* calculations. The doping is achieved by substituting two or more Mo atoms by TM atoms of the $3d$ series. Additionally, the effect of codoping on the 2D MoS$_2$ by cation-cation and cation-anion pairs is also investigated. Our results demonstrate that the TM doping of 2D MoS$_2$ leads to a significant reduction of the energy gap and the appearance of magnetic features whose major characteristic is the ferromagnetic coupling of the TM dopants. The latter is found to be significantly enhanced by codoping as demonstrated by codoping with (Co,Cu), (Ni,Cu), (Mn,Cu), and (Mn,Sb) codopant pairs.

I. INTRODUCTION

Transition metal dichalcogenides (TMDs) have been the subject of great current interest. The single layer MX$_2$ TMDs [M and X denoting the transition metal (TM) and the chalcogen atoms, respectively] were found to exhibit adsorption and photoluminescence properties which differ dramatically as compared to the corresponding bulk values [1]. This was attributed to confinement effects resulting from the decoupling of the adjacent MX$_2$ layers and their mutual s-p_z orbital interactions (z axis perpendicular to the 2D layer) leading to the widening of the band gap. Furthermore, nearest-neighbor interlayer d-d interactions producing a splitting within the d_{z^2} subband are also eliminated.

An important feature shared by all of the MX$_2$ compounds is the fact that the metal s-p bands lie well above the Fermi level. This is caused by the strong overlap and covalent-bonding effects between the metal and chalcogen s-p orbitals. This results in the formation of metal-chalcogen bonding and antibonding s-p states. The energy separation between the bonding and antibonding s-p orbitals is generally referred to as the σ-$\sigma^\star$ gap within which the TM(d) states are usually located [2].

Despite the plethora of reports on the electronic structure properties of the single layer TMDs it was only recently that a few works have been reported on their magnetic features [3–6]. To the best of our knowledge, no magnetism has been experimentally observed in the 2D's MoS$_2$ and WS$_2$. Magnetism has been confirmed in the 2D's VS$_2$ and VSe$_2$ [7] and in metal intercalated TMDs M$_x$NbSe$_2$, (M: Fe and Cu [8]). However, the structural analog of graphene with the single layer TMDs [9–11] has led to the search for magnetism in doped TMDs of zero-dimensional (0D) [9,10], one-dimensional (1D) [12], and two-dimensional (2D) [4–6,13–15] form.

In 0D and 1D MoS$_2$, the magnetic features were attributed to the presence of edge spins on the prismatic edges of the nanosheets where the terminating atoms are unsaturated. In the case of 2D MoS$_2$ the appearance of magnetism was found to be related to the presence of defects (including structural defects and/or adatoms and/or impurities). However, sulfur vacancy (O_S) and MoS divacancy (O_{MoS}) were found not to induce any magnetism in contrast to the triple vacancy (O_{MoS_2}) which induces magnetic features [13]. The substitution of a S atom by atoms of complete d band (Pd and Au) was found not to lead to magnetic polarization except for a slight modification of the DOS near the Fermi energy [15]. On the other hand, substitution of a S atom by atoms with incomplete d band atoms (Fe and V) was found to induce spin polarization and significant modification of the states near the band edges [15]. Magnetism was also found resulting from the adsorption of various adatoms (H-, B-, C-, N-, F-) [14] and (C, Co, Cr, Fe, Ge, Mn, Mo, Ni, O, Pt, S, Sc, Si, Ti, V, W) [13]) on 2D MoS$_2$.

It is only very recently that the effect on TMD's magnetism upon cation substitution with magnetic impurities has been investigated. In particular, Mishra *et al.* [4] investigated the long-range ferromagnetic ordering in fairly diluted Mn doped (less than 5%) 2D MoS$_2$, MoSe$_2$, MoTe$_2$, and WS$_2$ within the DFT/SGGA+U (density functional theory–spin polarized generalized gradient approximation and Hubbard-U parametrization). Similarly, Cheng *et al.* [5] studied the magnetism of the MoS$_2$ monolayer doped with (6.25%) Mn, Fe, Co, Zn, Cd, and Hg within the DFT/SGGA+U approximation. According to Ref. [5], Fe and Co doping lead to an AFM ground state, while the doping with Mn, Zn, Cd, and Hg lead to a FM ground state. Ramasubramaniam and Naveh [6] compared results for the exchange coupling coefficient among Mn dopants in 2D MoS$_2$ as obtained within the DFT/PBE and the HSE functionals. They found noticeable differences only at the nearest neighbor (nn) dopant distances. In particular, they found FM coupling between Mn dopants and AFM spin polarization between the Mn dopants and their fist nn S anions.

---

[*]andriot@iesl.forth.gr
[†]madhu@ccs.uky.edu

The reported results indicate that structure relaxation appears to be a crucial factor in the development of magnetism as Jahn-Teller distortions destroying the C_{3v} lattice symmetry lead to the disappearance of magnetism [5]. Additionally, it has been found that the results show noticeable dependence on the cell size used in the computer simulations [4–6].

The discrepancies among the reported results and the proposed model justification of the magnetic features of the doped 2D MoS$_2$ urges for a re-examination of this system using accurate calculations employing larger unit cells. Such an investigation of the magnetism of the doped 2D TMDs would not only expand our understanding of the underlying physics but could potentially lead to the discovery of new phenomena and applications and, in particular, the possibility of technologically important tunable magnetic properties. Our present work addresses this timely issue by investigating whether the TMDs with a relatively large energy gap, such as MoS$_2$, can accommodate magnetic features on substitution with magnetic impurities of the 3d TMs.

II. COMPUTATIONAL DETAILS

In our computational procedure, we use the density functional theory (DFT) in the generalized gradient approximation (GGA) and the Perdew-Burke-Ernzerhof (PBE) [16] augmented by including Hubbard-U corrections (DFT/GGA+U formalism [17]) based on Dudarev's approach [18] as implemented in the Vienna Ab-initio Simulation Package (VASP) [19–21]. The projected augmented wave (PAW) potential [20,21] is used to describe the core electrons. Calculations were performed at the Γ point using a kinetic plane wave cutoff energy of 450 eV. All calculations are self-consistent and were carried out using a total energy convergence criterion of 10^{-5} eV. The geometric structures in all cases were optimized without any symmetry constraints and checked for their stability. The volume of the surface unit cell was kept constant while allowing the full relaxation of all the atomic positions. A common U value, $U_d = 5.5$ eV, was assigned to all the 3d impurities, while no U parametrization was used for the impurity free MoS$_2$ single layer because the obtained value for the band gap with $U = 0$ eV was found to be in very good agreement with existing reports.

A unique and relatively accurate U parametrization could be possible if the chosen U parameters for the cation d and anion p orbitals would have been fitted to two experimental properties of the material, namely the band gap and a spectral or structural property [17,22]. Due to the lack of available experimental data, we limited ourselves to U values for the 3d impurities to those commonly used in electronic *ab initio* calculations for TMs and TM oxides (TMOs). However, results obtained for $U_d = 0.0$ eV, $U_d = 2.5$ eV, and $U_d = 5.5$ eV are also presented for comparison.

We consider the single layer MoS$_2$ in the 1H structure extended along the xy plane. This is simulated by a relatively large 192 atom supercell suitable for a random distribution of impurity atoms in it. Periodic boundary conditions are applied in all three directions. The supercell is periodically repeated along the x and y directions, while along the z direction (taken to be perpendicular to the surface layer) vacuum regions of sufficient width are allowed on both sides of the MoS$_2$ layer.

III. RESULTS

We calculate the electronic band gaps for the pristine MoS$_2$ layer and in the presence of various defects. We find that the pristine MoS$_2$ exhibits a direct gap of 1.87 eV, in very good agreement with previous theoretical (DFT/SGGA and GW) and, surprisingly, experimental reports [2,4–6,23–28]. It is also found that the 2D MoS$_2$ gap is not affected if two S atoms are replaced by two Se atoms, in agreement with the results of Ref. [4]. On the other hand, and in agreement with Cheng *et al.* [5], the band gap is found to be significantly reduced in the presence of single S (O_S) or Mo (O_{Mo}) vacancies with values of 1.23 and 1.16 eV, respectively (see Fig. 1, left panel).

The TM impurity doped structures are obtained by substituting two nearby Mo atoms (i.e., two Mo atoms sharing a common S neighbor) in a 192 atom cell of the MoS$_2$ monolayer by two TM atoms of the 3d series of the periodic table (belonging to the same or different species) and letting the system structurally relax. To check the stability of all the structures considered, we have performed *ab initio* molecular dynamics using the VASP code in the micro canonical ensemble; i.e., molecular dynamics at a constant number of particles n, constant volume V, and constant free energy E. The structures were heated to 1000 K. The duration of simulations was 300 femtoseconds (fm) in each case. All the structures were found to be stable.

In analyzing our results obtained using $U_d = 5.5$ eV, it is observed that in all monodoped cases (both TM belonging to the same species) studied, the two TM impurities were found to exhibit identical magnetic moments μ_{TM}, exhibiting ferromagnetic (FM) coupling between them. Our results are in agreement with those of Mishra *et al.* [4] for Mn, Fe, and Co dopants at nn TM-TM distances. For the Mn-doped case we are also in agreement with the results of Ref. [5], but we disagree for the cases of Fe and Co dopants for which these authors find AFM ground states. The disagreement may be attributed to the different cell sizes employed in all these calculations and reflects the delicate dependence of the results on the computational details. This supports our choice of employing a much larger unit cell in our investigation in order to avoid interactions between intercell TMs.

As expected, it is also found that each μ_{TM} induces electron spin polarization on its nearby anions (S atoms) (see, for example, Ref. [29]) with the result that the total magnetic moment $\mu_{u\text{-cell}}$ is found to be either smaller or greater than $2\mu_{TM}$ (the sum of the magnetic moments of the two impurities). The former (and, correspondingly, the latter) case appears when the induced spin polarization on the anions leads to anion magnetic moments μ_S with directions antiparallel (and, correspondingly, parallel) to that of the TM impurities. As shown in the middle panel of Fig. 1, TM impurities of the early 3d series induce antiparallel magnetic moments on their nearby anions giving rise to an antiferromagnetic (AFM) order in their neighborhood with the only exception to this trend found for the Ti impurities. On the other hand, TM impurities of the late 3d series induce spin polarization on the nearest neighboring anions parallel to their own. This explains the pronounced $\mu_{u\text{-cell}}$ values found for these dopants. For example, Mo$_{62}$Ni$_2$S$_{128}$ exhibits ferromagnetism
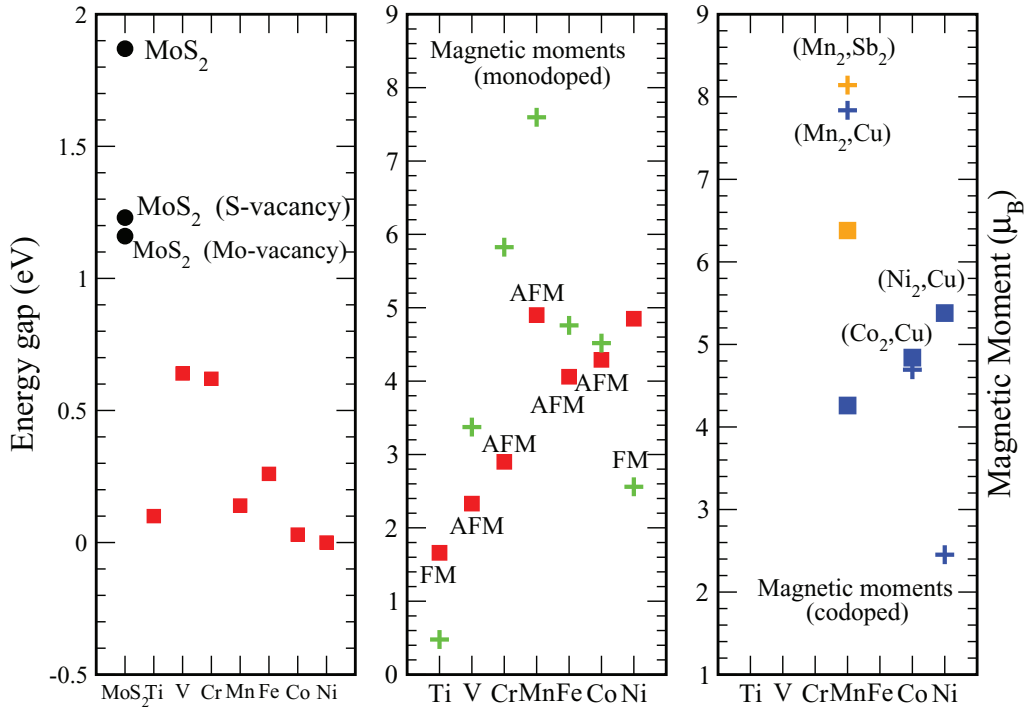
FIG. 1. (Color online) Energy gaps (left panel) and magnetic moments (middle and right panels) of single layer $Mo_{62}TM_2S_{128}$ with the TM taken from the $3d$ series. The middle (right) panel includes results for the monodoped (codoped) systems, respectively. In the left panel results for $Mo_{64}S_{128}$ and the defected systems: $Mo_{63}S_{128}$ and $Mo_{64}S_{127}$ are also presented. Defect-free and defected MoS_2 structures do not exhibit magnetic moments. In the middle panel, solid (red) squares denote the magnetic moment per unit cell (μ_{u-cell}) while (green) pluses denote the sum of the magnetic moments of the impurity TM atoms ($2\mu_{TM}$). In the right panel blue (solid square and plus symbols) indicates corresponding results for the MoS_2 systems codoped with (Mn_2Cu), (Co_2Cu), and (Ni_2Cu). The cationic-anionic codoping (Mn_2Sb_2) is shown in orange (solid square and plus symbols).

with $\mu_{u-cell} = 4.85\ \mu_B$ and $\mu_{Ni_1} = \mu_{Ni_2} = 1.279\ \mu_B$. Overall, as seen in Fig. 1 (middle panel), the total magnetic moment per unit cell varies linearly with the filling number of the d orbitals of the dopants with the exception of Mn. All our results for the magnetic moments are included in Fig. 1 (middle panel).

The dependence of the obtained results on the choice of the U_d parameter that is used for the TM dopants is shown in Fig. 2. In this, results analogous to those shown in Fig. 1 are shown for $U_d = 0.0$ and $U_d = 2.5$ along with the corresponding ones obtained with $U_d = 5.5$ eV. As it is apparent from the right panel of Fig. 2, the variation with U_d of the magnetic moment of the TM dopant, $\mu_{TM}(U_d)$, along the series of the $3d$ TM dopants follows the same trend; despite the increase in the absolute values of $\mu_{TM}(U_d)$'s as U_d increases, their variation exhibits the well known dependence on the d-band filling factor [30,31]. On the other hand, it is observed from the left panel of Fig. 2 that the variation with U_d of the total magnetic moment of the unit cell, $\mu_{cell}(U_d)$, follows that of $\mu_{TM}(U_d)$ only for $U_d = 0.0$ eV. As U_d takes nonzero values, $\mu_{cell}(U_d)$ increases with U_d in going from the left to the right side along the series of the $3d$ TM series. The latter behavior can be attributed to the delicate interplay between three main processes which take place upon the TM substitution, namely: (i) the increase of $\mu_{TM}(U_d)$ as U_d increases; (ii) the development of induced spin polarization on the 1 nn anions to the TM dopants and the formation of anion magnetic moments, $\mu_{anion}(U_d)$, on the anions; and (iii)

the alignment of the direction of $\mu_{anion}(U_d)$ relative to that of $\mu_{TM}(U_d)$ (see sections below).

An observation worth mentioning is shown in Fig. 3. In this figure, we present the variation with U_d of the range of the bond lengths of the bonds formed between the TM dopant and its 1 nn S anions. Maximum (correspondingly minimum)
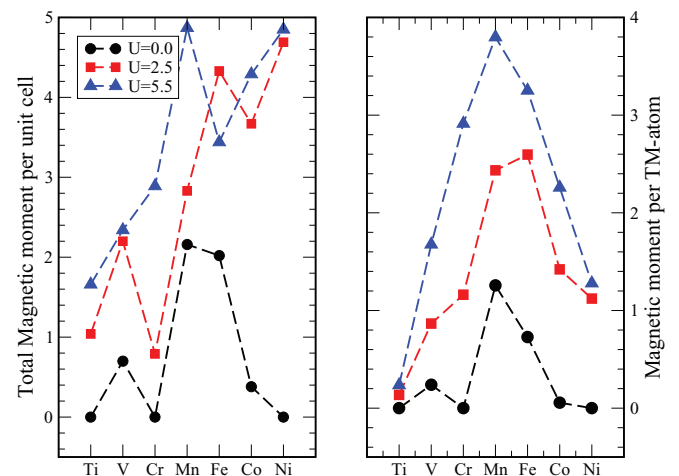

FIG. 2. (Color online) Variation with U_d of the total (per cell) magnetic moment $\mu_{cell}(U_d)$ and that of the magnetic moments $\mu_{TM}(U_d)$ of the TM-substitutional impurities in MoS_2 for $U_d = 0.0$, 2.5, and 5.5 eV.
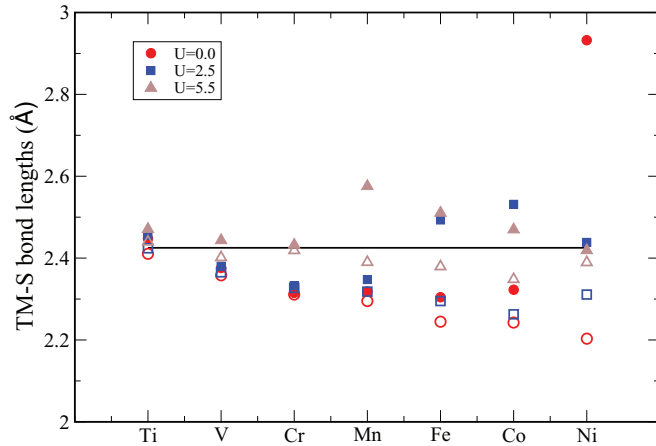
FIG. 3. (Color online) Variation with U_d of the range of the bond lengths of the bonds formed between the TM-substitutional impurity and its 1 nn S anions in MoS$_2$. Maximum (correspondingly minimum) bond lengths are indicated by filled (correspondingly unfilled) symbols for $U_d = 0.0$, 2.5, and 5.5 eV. The straight line indicates the unrelaxed TM-S bond lengths.

bond lengths are indicated by filled (correspondingly unfilled) symbols for $U_d = 0.0$, 2.5, and 5.5 eV. It can be seen that there is an absence of a clear correlation between the variation with U_d of the magnetic moments and the corresponding variation of the bond lengths. This means that the increase in $\mu_{\text{TM}}(U_d)$ as the result of the exchange splitting imposed by the U_d parameter is stronger than the crystal splitting resulting from

the hybridization of the anion p orbitals with those of the TM-dopant d orbitals.

Despite the quantitative changes in the magnetic moments that result from the variation of the U_d parameter, the picture of the induced spin polarization by the magnetic dopants on their 1 nn S anions does not change. For this reason, the discussion that follows in the next sections will only refer to the results obtained using $U_d = 5.5$ eV.

IV. DISCUSSION

Further insight into the correlation between the d-orbital filling of the TM doped MoS$_2$ and its electronic band gap and magnetic properties can be gained by a closer examination of the electronic structure evolution of the doped system.

A. Monodoped systems

Upon substituting two Mo atoms with Ti atoms (early $3d$ TM), the system develops flat impurity bands within the gap and, as a result, the band gap is reduced to 0.10 eV as shown in the band structure and DOS plots presented in Fig. 4 (top panels). The case of Mo$_{62}$Ti$_2$S$_{128}$ is an interesting one due to the fact that the atomic orbital (AO) energies of Ti(s) and Ti(d) orbitals are very close to the corresponding ones of Mo(s) and Mo(d) orbitals [32]. So no appreciable change in the hybridization processes (namely in the energies of the bonding and antibonding orbitals formed in the defect-free MoS$_2$) can be expected and, correspondingly, no appreciable change in the band gap. Instead, we find a large reduction in the gap value. This may be, in part, due to the differences in the Ti-S
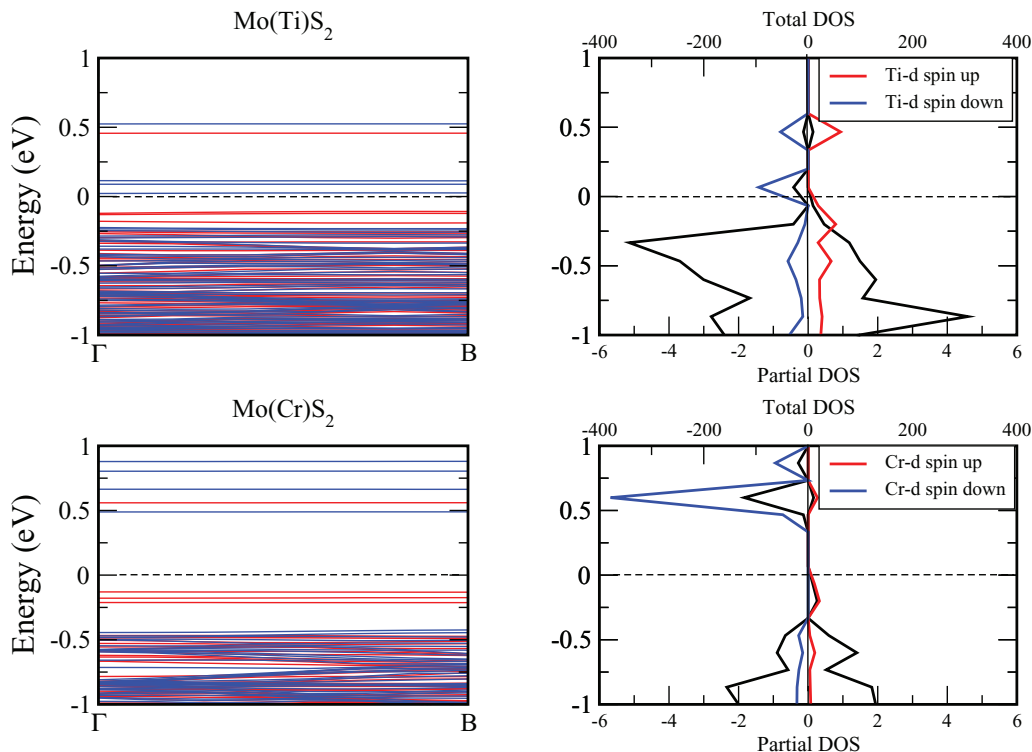

FIG. 4. (Color online) Band structure and DOS for Mo$_{62}$Ti$_2$S$_{128}$ (top) and Mo$_{62}$Cr$_2$S$_{128}$ (bottom) obtained using $U_d = 5.5$ eV. Spin-up and spin-down lines are indicated in red and blue, respectively, in band structure and DOS plots. In the DOS plots, the total DOS are shown in black. The Fermi level E$_F$ is at zero.

and Mo-S orbital couplings, but can largely be attributed to the different d and s filling factors of Mo and Ti valence d and s orbitals, respectively. To be more specific, the Ti atom ($3d^2 4s^2$) having four less valence electrons than the Mo atom ($3d^7 4s^1$) leaves some of the Ti-S bonds incomplete, thus resulting in the formation of defect bands in the gap. We find a magnetic moment of 1.66 μ_B per unit cell and 0.239 μ_B per Ti atom for $Mo_{62}Ti_2S_{128}$.

In view of the discussion about the $Mo_{62}Ti_2S_{128}$ it is reasonable to expect that substitution of two Mn atoms with two Cr atoms would not lead to the formation of defect bands since the Cr atom belongs to the same (VI-B) column of the periodic table and has the same valence electron configuration as Mo. However, upon the Cr substitution, the system exhibits a reduced energy gap of 0.62 eV as demonstrated in the band structure and DOS plots shown in Fig. 4 (lower panels). This can be attributed to the presence of impurity bands inside the gap caused by the difference in the AO energies of Mo and Cr [32]. This results in the formation of bonding and antibonding states between the Cr-S (s-p) orbitals at different energy levels than those formed between Mo-S (s-p) ones. Furthermore, the splitting of the lower Cr d_{z^2} and $d_{x^2-y^2}$ orbitals adds additional impurity levels in the gap. Finally, structural changes developed in the neighborhood of the Cr atoms due to the shorter Cr-S bonds could provide additional defect states. The study of both $Mo_{62}Ti_2S_{128}$ and $Mo_{62}Cr_2S_{128}$ systems indicates that the gap and the magnetic properties of the doped MoS$_2$ show a sensitive dependence on the d-band filling, the presence of S dangling bonds, the AO energies of the doping TM as well as the structural defects (defect states).

Next, we calculate the band structure of the $Mo_{62}TM_2S_{128}$ systems in which the TM is one of the $3d$ series. Recalling that in going from the early TMs to the late ones of the $3d$ series (similarly for the $4d$ and $5d$ series), the TM(d) AO energy shifts to lower energy [32], and only Ti(d) and W(d) have AO energies that are close to the AO energy of Mo(d). Furthermore, Mo(s), Ti(s), and W(s) AO energies are almost equal. This explains the similarity in the band structures of MoS$_2$ and WS$_2$ as Mo and W have the same valence electron configurations.

Examining the variation of the TM(d) AO energies with the atomic number, and considering the fact that the TM(s) AO energies remain almost unchanged as the atomic number is varied, one can conclude that the substitution of Mo atoms with $3d$ TMs in 2D MoS$_2$ results in the formation of new bonding and antibonding states between TM(d) and S(p) orbitals with the orbital energies spanning an energy range that is extended over the gap range of the 2D MoS$_2$. This is confirmed by our *ab initio* calculations.

The substitution of two Mo atoms by $3d$ TMs thus leads to a reduction in the energy gap of MoS$_2$ which, with the exception of Ti, appears to be more pronounced as we go from the left of the periodic table to the right along the $3d$ series (see the left panel of Fig. 1). It is worth noting that only at the very end of the $3d$ series (e.g., doping with Co and Ni atoms) that we find the occurrence of metallicity. At the same time, the doped systems show magnetic features exhibiting magnetic moments which increase with the d-band filling of the TM dopant.

B. Codoped systems

In order to further explore the defect induced magnetic enhancement in 2D MoS$_2$, we investigated the effect of codoping. As demonstrated in our recent works, significant enhancement in the ferromagnetic coupling (FMC) among the magnetic dopants can be achieved for the diluted magnetic semiconductors (DMSs) and transition metal oxides (TMOs) by codoping [29,33–42]. We attributed this enhancement to successive local spin correlations of ferromagnetic type which act in opposition to the AFM superexchange coupling. Based on these investigations, we investigated the codoping of the 2D-MoS$_2$ monolayer using pairs of cationic-cationic as well as cationic-anionic codopants.

As a first example we consider the effects of codoping with Ni and Cu. After obtaining the $Mo_{62}Ni_2S_{128}$ structure by monodoping, we substituted an additional Mo by a Cu atom in such a way as to have the Cu atom become a common first nearest neighbor (1 nn) cation to both the Ni dopants forming a bipartite Ni-Cu-Ni segment. Upon relaxation, we find that $\mu_{\text{u-cell}}$ increases (from 4.85 μ_B of the monodoped case) and takes the value of $\mu_{\text{u-cell}} = 5.38\mu_B$, while the magnetic moments of the Ni atoms do not change appreciably as compared to the monodoped case. The relaxation of $Mo_{61}Ni_2CuS_{128}$ leads to local deformation around the Cu atom as indicated in Table I.

Similar behavior and enhancement of $\mu_{\text{u-cell}}$ of the corresponding monodoped $Mo_{62}Co_2S_{128}$ system is also obtained when codoped with Cu, although Co, in contradistinction to Ni, induces rather an opposite spin polarization to its 1nn anions. In this case $\mu_{\text{u-cell}}$ increases from 4.29 μ_B (monodoped case) to 4.84 μ_B while no substantial change is observed in the values of μ_{Co}'s (see Table I). The increase of $\mu_{\text{u-cell}}$ upon codoping in both $Mo_{61}Ni_2CuS_{128}$ and $Mo_{61}Co_2CuS_{128}$ can be mainly attributed to the spin polarization induced on the Cu atom and its 1nn anions. This effect is stronger in the case of the codopant pair (Ni,Cu) in which all spin polarizations are aligned along the same direction, while in the case of (Co,Cu) we find polarizations that are opposite to the codopant. In Fig. 5, we show the spin densities of the codoped $Mo_{61}Co_2CuS_{128}$ system. Although in this example the contribution of Cu is small, its presence has the effect of further stabilizing the FM phase despite the considerable antiparallel spin polarization induced mainly on the surrounding anions.

Interestingly, in contradistinction to the $Mo_{61}Ni_2CuS_{128}$ and $Mo_{61}Co_2CuS_{128}$ cases, in $Mo_{61}Mn_2CuS_{128}$ the spin polarization of the Cu atom as well as that of the 1 nn anions of the Mn atoms is antiparallel to that of the Mn atoms. This leads to a small reduction of $\mu_{\text{u-cell}}$ upon codoping (becoming 4.26 μ_B) as compared to the corresponding value of the monodoped case (4.87 μ_B) and despite the fact that the magnetic moments μ_{Mn} of the Mn atoms increase only slightly upon codoping (from 3.798 to 3.913 μ_B).

An interesting case was found when we used substitutional codopants of the cation-anion pairs, namely two neighboring (Mn,Sb) pairs (with the Mn atoms sharing a common S atom, see Fig. 6). Upon relaxation, the system exhibits a significant ferromagnetic enhancement compared to the monodoped $Mo_{62}Mn_2S_{128}$ system (exhibiting $\mu_{\text{u-cell}} = 4.87$ μ_B). In the codoped $Mo_{62}Mn_2Sb_2S_{126}$ system, the μ_{Mn}'s (of 4.071 μ_B each) are ferromagnetically coupled resulting in

TABLE I. Energy gap and magnetic moment (per unit cell and per impurity TM atom) for the codoped single layer materials $Mo(TM_2^\alpha, TM^\beta)S_2$ and $Mo(TM_2^\alpha, Sb_2)S_2$ (with TM^α and TM^β taken from the $3d$ series). The results were obtained within the DFT/SGGA+U level of approximation ($U = 5.5$ eV). Results for $\mu_{u\text{-cell}}$ in the monodoped case are shown in parentheses. In the last column we include representative bond lengths (in the neighborhood of the dopants) which are expressed as percentage changes with respect to the average Mo-S bond length (far from the dopants). The bond length referred to is specified by completing the corresponding lattice segment in parentheses.

System	E_{gap} (eV)	μ_{imp} (μ_B/unit cell)	μ_{imp} (μ_B/imp-TM atom)	TM_{imp}-S bonds compared to Mo-S ones
$Mo_{61}Ni_2CuS_{128}$	0.00	5.38 (4.85)	1.222 (Ni)	bonds: Ni-S(-Cu) $\in [-1.2, -0.8]\%$
			1.231 (Ni)	bonds: Cu-S(-Ni) $\in [-2.4, +7.0]\%$
			0.268 (Cu)	bonds: Cu-S(-Mo) $\in [-3.4, +1.0]\%$
$Mo_{61}Mn_2CuS_{128}$	0.00	4.26 (4.87)	3.914 (Mn)	bonds: Mn-S(-Cu) $\in [-1.4]\%$
			3.923 (Mn)	bonds: Cu-S(-Mo) $\in [-2.7]\%$
			-0.262 (Cu)	bonds: Cu-S(-Mn) $\in [+19.0]\%$
$Mo_{61}Co_2CuS_{128}$	0.00	4.84 (4.29)	2.347 (Co)	bonds: Co-S(-Cu) $\in [-1.0]\%$
			2.347 (Co)	bonds: Cu-S(-Co) $+8.5\%$
			0.029 (Cu)	bonds: Mo-S(-Cu) -1.3%
$Mo_{62}Mn_2Sb_2S_{126}$	0.14	6.38 (4.87)	4.071 (Mn)	bonds: Mn-S(-Mn) $+10.6\%$
			4.071 (Mn)	bonds: Mn-Sb(-Mo) $+6.3\%$
			-0.056 (Sb)	

an increase in $\mu_{u\text{-cell}}(=6.38\ \mu_B)$ although this is significantly reduced (with respect to the sum of μ_{Mn}'s) due to antiparallel spin polarization induced on the 1 nn (to the codopants) anions.

C. Successive spin-induced polarization versus superexchange

A key issue underlying the magnetic coupling among the magnetic dopants in MoS$_2$ and, in general in many other DMSs, is the induced spin polarization by the magnetic dopants on their nearest neighbor anions, namely the S anions in the case of MoS$_2$. As pointed out and demonstrated by us in a series of recent reports [29,35–37,39,40,43], the spin-polarized anions which are first nn to a specific magnetic dopant, say TM_1, dictate the spin polarization of another dopant, say TM_2, which shares the same anion with TM_1. This picture of successive spin-induced correlations is a local process which becomes more pronounced in the case of codoping. It is opposed to the superexchange interaction that could
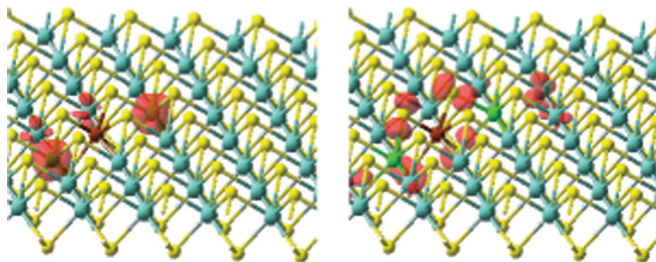
be developed among the magnetic dopants. Depending on the strength of the induced polarization on the anions it can lead to the ferromagnetic coupling among the codopants even at dopant concentrations smaller than the percolation threshold [29,35–37,39,40,43].

Mishra *et al.* [4] invoked this type of successive spin-induced correlation in order to justify the ferromagnetic coupling among the Mn dopants in MoS$_2$. As double exchange is ruled out due to the AFM coupling between Mn and its first nn S atoms [4], the contribution of the superexchange interaction has to be weaker than that of the induced spin polarization. It should be noted, however, that if it so happens that the first nn anions to the dopants are spin polarized in the same direction as the polarizing dopants, then additional contribution to the FM coupling can be developed through double exchange.

V. CONCLUSION

In summary, we have investigated the effect of substitutional monodoping and codoping on the electronic and
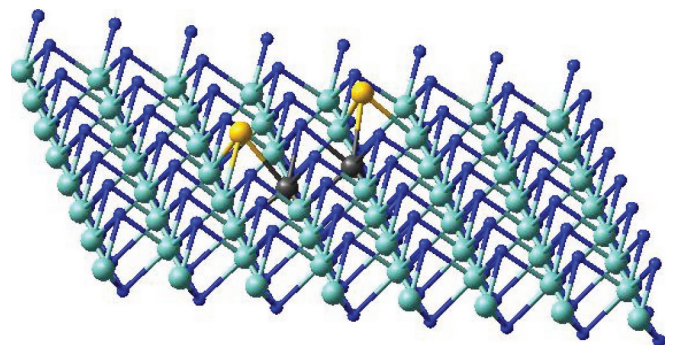

FIG. 5. (Color online) Electron spin densities in codoped $Mo_{61}Co_2CuS_{128}$ system. The left panel shows the positive spin density in the codoped system. The right panel shows the induced negative spin density. As seen in the figure, the majority of the positive spin density is localized on the Co atoms. In the left panel we used an isosurface of $0.05\ e/\text{Å}^3$, while for the right panel we used an isosurface of $0.02\ e/\text{Å}^3$ for clarity. The Co and Cu atoms are indicated by green and brown color, respectively.

FIG. 6. (Color online) Relaxed structure of $Mo_{62}Mn_2Sb_2S_{126}$. Mo, S, Mn, and Sb atoms are denoted by cyan, blue, black, and orange color, respectively.

magnetic properties of MoS_2. We used cationic dopants of the $3d$ TMs and Sb atoms as anionic dopants. Our results indicated that monodoping leads to a reduction in the electronic gap of MoS_2 which becomes more pronounced as we move to the right of the $3d$ TM series in the periodic table. At the same time, the monodoped systems show magnetic features exhibiting magnetic moments which increase with the d-band filling of the TM dopant. As in the case of DMSs and TMOs, we find that codoping can lead to an enhancement of the magnetism over monodoping as a result of the synergistic action of the codopants; this is realized through the codopants which introduce ferromagnetic contributions in the form of successive local spin correlations that act to oppose the superexchange coupling. (see, for example, Ref. [29] and references therein). The synergistic action of the codopants depends on their pairing as well as the interaction with the host material which determine their ability to spin polarize their 1nn anions in either a parallel or antiparallel way relative to their own polarization.

[1] T. Li and G. Galli, J. Phys. Chem. C **111**, 16192 (2007).

[2] M. Chhowalla, H. S. Shin, G. Eda, L. Li, K. P. Loh, and H. Zhang, Nat. Chem. **5**, 263 (2013).

[3] M. Xu, T. Liang, M. Shi, and H. Chen, Chem. Rev. **113**, 3766 (2013).

[4] R. Mishra, W. Zhou, S. J. Pennycook, S. T. Pantelides, and J.-C. Idrobo, Phys. Rev. B **88**, 144409 (2013).

[5] Y. C. Cheng, Z. Y. Zhu, W. B. Mi, Z. B. Guo, and U. Schwingenschlogl, Phys. Rev. B **87**, 100401(R) (2013).

[6] A. Ramasubramaniam and D. Naveh, Phys. Rev. B **87**, 195201 (2013).

[7] Y. D. Ma, Y. Dai, M. Guo, C. W. Niu, Y. T. Zhu, and B. B. Huang, ACS Nano **6**, 1695 (2012).

[8] Y. Koh, S. Cho, J. Lee, L.-X. Yang, Y. Zhang, C. He, F. Chen, D.-L. Feng, M. Arita, K. Shimada, H. Namatame, M. Taniguchi, and C. Kim, Jpn. J. Appl. Phys. **52**, 10MC15 (2013).

[9] J. Zhou, Q. Wang, Q. Sun, X. S. Chen, Y. Kawazoe, and P. Jena, Nano Lett. **9**, 3867 (2009).

[10] C. N. R. Rao, H. S. S. Ramakrishna, K. S. Subrahmanyam, and U. Maitra, Chem. Sci. **3**, 45 (2012).

[11] A. H. C. Neto and K. Novoselov, Rep. Prog. Phys. **74**, 082501 (2011).

[12] R. Shidpour and M. Manteghian, Nanoscale **2**, 1429 (2010).

[13] C. Ataca and S. J. Ciraci, Phys. Chem. C **115**, 13303 (2011).

[14] J. G. He, K. C. Wu, R. J. Sa, Q. H. Li, and Y. Q. Wei, Appl. Phys. Lett. **96**, 082504 (2010).

[15] J. D. Fuhr, A. Saul, and J. O. Sofo, Phys. Rev. Lett. **92**, 026802 (2004).

[16] J. P. Perdew, K. Burke, and M. Ernzerhof, Phys. Rev. Lett. **77**, 3865 (1996).

[17] A. N. Andriotis, G. Mpourmpakis, S. Lisenkov, R. M. Sheetz, and M. Menon, Phys. Status Solidi B **250**, 356 (2013).

[18] S. L. Dudarev, G. A. Botton, S. Y. Savrasov, C. J. Humphreys, and A. P. Sutton, Phys. Rev. B **57**, 1505 (1998).

[19] G. Kresse and J. Hafner, Phys. Rev. B **47**, 558 (1993).

[20] G. Kresse and D. Joubert, Phys. Rev. B **59**, 1758 (1999).

[21] P. E. Blöchl, Phys. Rev. B **50**, 17953 (1994).

[22] P. Khatri and M. N. Huda, Comput. Mater. Sci. **81**, 290 (2014).

[23] D. Xiao, G. B. Liu, W. Feng, X. Xu, and W. Yao, Phys. Rev. Lett. **108**, 196802 (2012).

[24] L. F. Mattheiss, Phys. Rev. B **8**, 3719 (1973).

[25] K. F. Mak, C. Lee, J. Hone, J. Shan, and T. F. Heinz, Phys. Rev. Lett. **105**, 136805 (2010).

[26] A. Splendiani, L. Sun, Y. Zhang, T. Li, and J. Kim, Nano Lett. **10**, 1271 (2010).

[27] E. S. Kadantsev and P. Hawrylak, Solid State Commun. **152**, 909 (2012).

[28] S. Lebegue and O. Eriksson, Phys. Rev. B **79**, 115409 (2009).

[29] A. N. Andriotis and M. Menon, Phys. Rev. B **87**, 155309 (2013).

[30] N. Papanikolaou, N. Stefanou, R. Zeller, and P. H. Dederichs, Phys. Rev. B **46**, 10858 (1992).

[31] K. Sato, L. Bergqvist, J. Kudrnovský, P. H. Dederichs, O. Eriksson, I. Turek, B. Sanyal, G. Bouzerar, H. Katayama-Yoshida, V. A. Dinh, T. Fukushima, H. Kizaki, and R. Zeller, Rev. Mod. Phys. **82**, 1633 (2010).

[32] W. A. Harrison, *Elementary Electronic Structure* (World Scientific, Singapore, 1999).

[33] A. N. Andriotis, M. Menon, R. M. Sheetz, and L. Chernozatonskii, Phys. Rev. Lett. **90**, 026801 (2003).

[34] A. N. Andriotis, R. M. Sheetz, E. Richter, and M. Menon, Europhys. Lett. **72**, 658 (2005).

[35] A. N. Andriotis, R. M. Sheetz, and M. Menon, J. Phys.: Condens. Matter **22**, 324210 (2010).

[36] A. N. Andriotis, S. Lisenkov, and M. Menon, J. Phys. Condens. Matter **23**, 086004 (2011).

[37] A. N. Andriotis and M. Menon, Phys. Status Solidi B **248**, 2032 (2011).

[38] N. N. Lathiotakis, A. N. Andriotis, and M. Menon, Phys. Rev. B **78**, 193311 (2008).

[39] S. Lisenkov, A. N. Andriotis, R. M. Sheetz, and M. Menon, Phys. Rev. B **83**, 235203 (2011).

[40] A. N. Andriotis and M. Menon, J. Phys. Condens. Matter **24**, 455801 (2012).

[41] A. N. Andriotis, R. M. Sheetz, and M. Menon, J. Phys.: Condens. Matter **17**, L35 (2005).

[42] A. N. Andriotis, R. M. Sheetz, N. N. Lathiotakis, and M. Menon, Int. J. Nanotechnol. **6**, 164 (2009).

[43] S. Lisenkov, A. N. Andriotis, and M. Menon, Phys. Rev. Lett. **108**, 187208 (2012).